

# Manifestation of pseudogap in ab-plane optical characteristics

J. Hwang<sup>1</sup>, J. Yang<sup>1</sup>, J. P. Carbotte<sup>1,2</sup> and T. Timusk<sup>1,2</sup>

<sup>1</sup>Department of Physics and Astronomy, McMaster University, Hamilton, Ontario L8S 4M1, Canada

<sup>2</sup>The Canadian Institute for Advanced Research, Toronto, Ontario M5G 1Z8, Canada

E-mail: [jhwang@phys.ufl.edu](mailto:jhwang@phys.ufl.edu)

**Abstract.** A model in which a gap forms in the renormalized electronic density of state (DOS) with missing states recovered just above the pseudogap  $\Delta_{pg}$ , is able to give a robust description of the striking, triangular like, peak seen in the real part of the optical self-energy of underdoped cuprates. We use this model to explore the effect of the pseudogap on the real part of the optical conductivity and on the partial sum rule associated with it. An important result is that the optical spectral weight redistributes over a much larger frequency window than it does in the DOS.

PACS numbers: 74.25.Gz, 74.62.Dh, 74.72.Hs

## 1. Introduction

Cuprate superconductors undergo considerable change in their electronic structure as a function of doping. In the overdoped regime there is evidence that Fermi liquid theory applies. However, as the doping is reduced through the optimum and then underdoped regime, a non-Fermi liquid state evolves which is characterized by the formation of a pseudogap[1, 2, 3, 4, 5, 6, 7, 8, 9, 10, 11, 12]. There is as yet no consensus as to the correct microscopic understanding of the pseudogap state. There is evidence that it corresponds to the formation of preformed Cooper pairs[4] at some new characteristic temperature  $T^*$  above the superconducting  $T_c$ . Superconductivity sets in at the temperature where phase coherence among the preexisting pairs occurs. Only then does the system acquire long range order. Another prominent possibility for the pseudogap is competing order[13, 14, 15, 16, 17, 18, 19, 20, 21, 22, 23, 24, 25, 26, 27, 28] such as d-density wave formation. On the other hand, from a phenomenological point of view many experimental findings, in the pseudogap region of the cuprate phase diagram, can be understood in a model which corresponds to a reduction of the electronic density of state in the vicinity of the Fermi energy over an energy region ( $\Delta_{pg}$ ) which sets the pseudogap scale. An important concept in such a characterization of the pseudogap is its variation with temperature. At zero temperature there is a full gap of order  $\Delta_{pg}$  which fills in with increasing temperature but does not change its magnitude[7, 12]. The pseudogap temperature ( $T^*$ ) corresponds to compete filling rather than closing *i.e.*  $\Delta_{pg} \rightarrow 0$ .

Recently more details about the temperature evolution of the pseudogap have emerged from angle-resolved photoemission (ARPES) experiments which have been interpreted in term of Fermi arcs[7]. Below  $T^*$  a full pseudogap opens up, but only on a small region of the Fermi surface near the antinodal direction. The rest of the Fermi surface, called the Fermi arc, remains ungaped. Experiments have shown that the length of the Fermi arc centered in the nodal direction is proportional to the reduced temperature  $t = T/T^*$  and vanishes at  $T = 0$  at which point the entire Fermi surface is fully gaped. The existence of a full gap in the electronic density of state at  $T = 0$  is consistent with many other experiments in particular specific heat. It also has implications for the behavior of the in-plane optical conductivity.

It has recently been pointed[29] out that the sharp triangular like cap observed in the real part of the optical self-energy seen in underdoped samples of  $\text{Bi}_2\text{Sr}_2\text{CaCu}_2\text{O}_{8+\delta}$  (Bi-2212)[30, 31] and orthoII  $\text{YBa}_2\text{Cu}_3\text{O}_{6.5}$  ( $\text{YBCO}_{6.5}$ )[32] follows directly from the opening of a full pseudogap with the lost electronic density of states below  $\Delta_{pg}$  recovered in the region just above it. This represents a clear signature of pseudogap behavior in optical spectroscopy. In this paper we consider the implication of such a phenomenological model on optical properties.

The paper is structured as follows. In section II we introduce the generalized Drude model for the optical conductivity which relates it to an optical self-energy,  $\Sigma^{op}(\omega)$ . We also summarize the data for the real part of  $\Sigma^{op}(\omega)$  on which our pseudogap model

is based and the distinct difference between underdoped and overdoped cases is noted and emphasized. Our theoretical model is introduced and compared with the data. In section III we deal with signatures of the pseudogap in the real part of the conductivity and partial sum rule. In section IV we conclude the paper with a summary of our findings.

## 2. Theoretical model

The optical conductivity  $\sigma(\omega)$  in a correlated electron system can be analyzed in terms of a generalized Drude form written as[29, 30]

$$\sigma(T, \omega) = \frac{i}{4\pi} \frac{\Omega_p^2}{\omega - 2\Sigma^{op}(T, \omega)}, \quad (1)$$

where  $T$  is temperature,  $\Omega_p$  is the plasma frequency and  $\Sigma^{op}(T, \omega) \equiv \Sigma_1^{op}(T, \omega) + i\Sigma_2^{op}(T, \omega)$  is the optical self-energy. The imaginary part of  $-2\Sigma^{op}(T, \omega)$  is equal to the optical scattering rate  $1/\tau^{op}(T, \omega)$  and the real part can be written in terms of an optical effective mass  $m^{*,op}(T, \omega)/m$  with  $\omega[m^{*,op}(T, \omega)/m - 1] \equiv -2\Sigma_1^{op}(T, \omega)$ . While the optical scattering rate and the mass renormalization  $\lambda^{op}(T, \omega)$  ( $1 + \lambda^{op}(T, \omega) \equiv m^{*,op}(T, \omega)/m$ ) defined here are not the same as those defined from the quasiparticle self-energy  $\Sigma^{qp}(T, \omega)$  they are related through the equation for the conductivity. Neglecting vertex corrections and taking zero temperature ( $T = 0$ ) for an isotropic system we have[33]

$$\sigma(\omega) = \frac{\Omega_p^2}{4\pi} \frac{i}{\omega} \int_0^\omega d\omega' \frac{1}{\omega + i/\tau_{imp} - \Sigma^{qp}(\omega') - \Sigma^{qp}(\omega - \omega')} \quad (2)$$

where we have also included the possibility of elastic impurity scattering through the constant scattering rate  $1/\tau_{imp}$ . The quasiparticle scattering rate is  $-2\Sigma_2^{qp}(\omega)$  and  $\omega[m^{*,qp}(\omega)/m - 1] \equiv -2\Sigma_1^{qp}(\omega)$  in complete analogy with the optical case. If a boson exchange theory is used to describe the interactions among electrons, the quasiparticle self-energy at  $T = 0$  is related to the electron-boson spectral density  $I^2\chi(\omega)$  through the equation[34, 35]

$$\Sigma^{qp}(\omega) = \int_0^\infty d\Omega I^2\chi(\Omega) \ln \left| \frac{\Omega - \omega}{\Omega + \omega} \right| - i\pi \int_0^{|\omega|} d\Omega I^2\chi(\Omega) \quad (3)$$

Here we need to generalize the formalism just given to include the possibility of an energy dependent renormalized electron density of state (DOS)  $N(\omega)$  which is defined as[35, 36, 37, 38, 39]

$$N(\omega) = \sum_{\underline{k}} \frac{-ImG(\underline{k}, \omega)}{\pi} \quad (4)$$

where  $G(\underline{k}, \omega)$  is the fully renormalized Green's function. In this case Eq. 3 needs modification and reads[34, 35, 36, 37, 38, 39]

$$\Sigma^{qp}(\omega) = 2\omega P \int_0^\infty d\omega' \tilde{N}(\omega') \int_0^\infty d\Omega \frac{I^2\chi(\Omega)}{\omega^2 - (\omega' + \Omega)^2} - i\pi \int_0^\omega d\Omega I^2\chi(\Omega) \tilde{N}(\omega - \Omega) \quad (5)$$

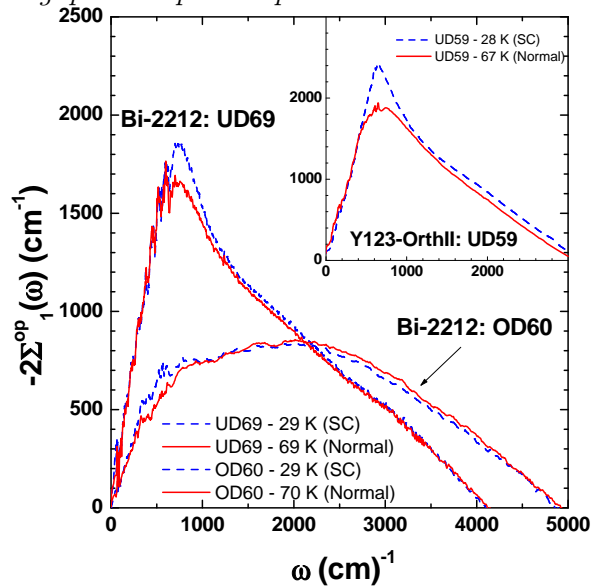


**Figure 1.** (color online) Minus twice the real part of the optical self-energy  $-2\Sigma_1^{op}(\omega)$  in units of  $\text{cm}^{-1}$  as a function of  $\omega$  also in  $\text{cm}^{-1}$  for an underdoped Bi-2212 with  $T_c = 69$  K (UD69) and an overdoped Bi-2212,  $T_c = 60$  K (OD60) at two temperatures; dashed (blue) in superconducting state and sold (red) in normal state. Shown in the inset are equivalent results for orthoII YBCO<sub>6.50</sub> which is underdoped with  $T_c = 59$  K (UD59).

Here  $\tilde{N}(\omega) \equiv [N(\omega) + N(-\omega)]/2$  is the symmetrized DOS. For the case with an energy dependent DOS the relationship between  $\Sigma^{qp}$  and  $\Sigma^{op}$  is more complicated than Eq. 2. There exists however simplified equation for  $\lambda^{op}(\omega)$  and  $1/\tau^{op}(\omega)$  which, while not exact, are sufficiently accurate for the present discussion. They are[35, 36, 37]

$$\lambda^{op}(\omega) = \frac{2}{\omega^2} \int_0^\infty d\Omega I^2 \chi(\Omega) P \int_0^\infty d\omega' \tilde{N}(\omega') \ln \left[ \frac{(\omega' + \Omega)^2}{(\omega' + \Omega)^2 - \omega^2} \right] \quad (6)$$

and

$$\frac{1}{\tau^{op}(\omega)} = \frac{2\pi}{\omega} \int_0^\infty d\Omega I^2 \chi(\Omega) \int_0^{\omega-\Omega} d\omega' \tilde{N}(\omega') \quad (7)$$

In this approximation, optical and quasiparticle quantities are related by  $\Sigma^{qp}(\omega) = d/d\omega[\omega\Sigma^{op}(\omega)]$  which can be verified through direct differentiation of Eq. 6 and 7 and comparison with Eq. 5. This relationship has been used in a recent comparison of high energy scales seen in optical data with those seen in ARPES[40] which measures directly the quasiparticle self-energy.

The exact microscopic origin of the pseudogap is not known. Here we model it as a gap in the fully renormalized electronic density of state  $\tilde{N}(\omega)$  of formula Eq. 4. Such a model has been used previously to analyze the specific heat[10, 11] in the underdoped regime of the high  $T_c$  cuprates and more recently applied to optics[29]. The motivating data is reproduced in Fig. 1 for the convenience of the reader. These sets of data, for the real part of the optical self-energy are presented for an in-plane underdoped sample of Bi-2212 with a  $T_c$  of 69 K, for another overdoped sample with  $T_c = 60$  K and in the inset

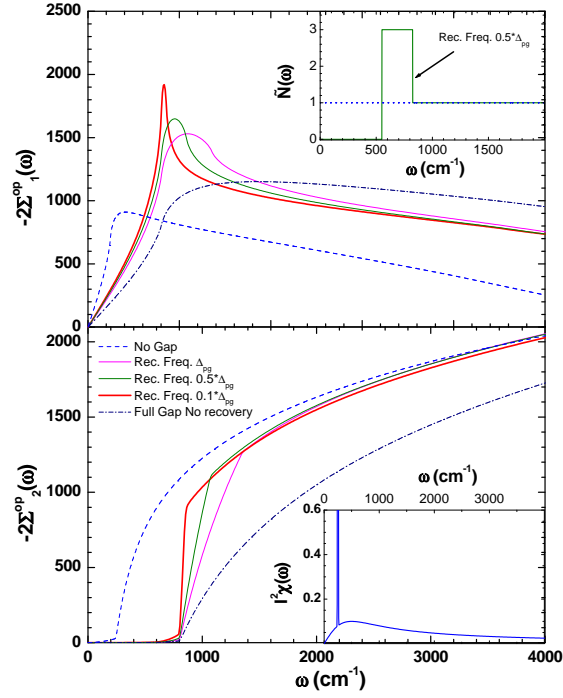


**Figure 2.** (color online) Model calculation of minus twice the real and imaginary parts of the optical self-energy  $-2\Sigma_1^{op}(\omega)$  (top frame) and  $-2\Sigma_2^{op}(\omega)$  (bottom frame) in  $\text{cm}^{-1}$  as a function of  $\omega$  also in  $\text{cm}^{-1}$ . All curves are based in the electron-boson spectral density shown in the inset lower frame. The dashed (blue) curve has no pseudogap while the dash-dotted has a pseudogap  $\Delta_{pg} = 550 \text{ cm}^{-1}$  but with no recovery of states in the self consistent density of state  $\tilde{N}(\omega)$ . The others have a recovery region right above  $\Delta_{pg}$  with conservation of total states applied. The recovered states are piled up in the region  $\Delta_{pg}$ ,  $(1/2)\Delta_{pg}$ , and  $(1/10)\Delta_{pg}$  for medium (purple), light (olive), and heavy (red), respectively. The inset in the upper frame shows the effective DOS  $\tilde{N}(\omega)$  in the case  $(1/2)\Delta_{pg}$ .

data on underdoped orthoII YBCO<sub>6.50</sub> with  $T_c = 59 \text{ K}$ . This material is particularly well-ordered with every second chain full and the others completely empty. In all cases two values of temperature are shown, one in the superconducting state (dashed blue curve) and the other in the normal state just above  $T_c$  (solid red curve). The difference between the behavior of underdoped and overdoped samples is striking and can be understood[29] as due to the opening of a pseudogap in the fully renormalized density of state  $\tilde{N}(\omega)$  of formula Eq. 4 which also determines the optical self-energy through equation Eq. 6 and Eq. 7. The prominent peak around  $750 \text{ cm}^{-1}$  seen in both underdoped materials which is absent in the overdoped case, can be traced to the opening of a gap in  $\tilde{N}(\omega)$  with lost states piled up in the energy region just above  $\omega = \Delta_{pg}$  as well as the existence of a prominent boson mode in the electron-boson spectral density  $I^2\chi(\Omega)$ . All three of the above conditions are needed.

Fig. 2 shows results of model calculations for minus twice the real part (top frame) and imaginary (bottom frame) part of the optical self-energy ( $\Sigma^{op}(\omega)$ ) for a system

with the electron-boson spectral density  $I^2\chi(\omega)$  shown in the inset of the lower panel. This model for the spectral density (note the prominent resonance peak at 31 meV) is motivated by an earlier study [32] of orthoII YBCO<sub>6.50</sub> in which  $I^2\chi(\omega)$  was fit to its measured optical scattering rate. What is different here is that we include a pseudogap in  $\tilde{N}(\omega)$  as well as a recovery region just above  $\Delta_{pg}$  where the lost states in  $\tilde{N}(\omega)$  are to be found so as to conserve states in the DOS. The blue dashed curve is for comparison and includes no pseudogap. The expressions for  $\lambda^{op}(\omega)$  and  $1/\tau^{op}(\omega)$  in this simple limit reduce to [34]

$$\lambda^{op}(\omega) = \frac{2}{\omega} \int_0^\infty d\Omega I^2\chi(\Omega) \left[ \frac{\Omega}{\omega} \ln \left| \frac{\Omega^2 - \omega^2}{\Omega^2} \right| + \ln \left| \frac{\Omega + \omega}{\Omega - \omega} \right| \right] \quad (8)$$

and [38, 41, 42]

$$\frac{1}{\tau^{op}(\omega)} = \frac{2\pi}{\omega} \int_0^\omega d\Omega (\omega - \Omega) I^2\chi(\Omega) \quad (9)$$

On comparing Eq. 9 with the imaginary part in Eq. 3, it is clear that for a simple delta function  $I^2\chi(\Omega) \equiv I_0\delta(\Omega - \Omega_E)$  which represents coupling to a single Einstein mode at  $\Omega_E$ , the optical scattering rate starts out of zero at  $\omega = \Omega_E$ , then rises according to the factor  $(\omega - \Omega_E)/\omega$  and reaches its saturated value of  $2\pi I_0$  only for  $\omega \gg \Omega_E$ . By contrast the quasiparticle scattering rate has a discontinuous jump out of zero at  $\omega = \Omega_E$  to its saturated value and remains at this constant value for all energies beyond this. This behavior for  $1/\tau^{op}(\omega)$  is seen in the (blue) dashed curve of Fig. 2 bottom frame. Because we have also included a background in  $I^2\chi(\omega)$  in addition to a prominent peak at  $\Omega_E = 250 \text{ cm}^{-1}$ , there are minor differences, including very small tails below the energy of the prominent peak in  $I^2\chi(\omega)$  shown in the inset. The dot-dashed (blue) curve includes a pseudogap  $\Delta_{pg} = 550 \text{ cm}^{-1}$  with the lost states in  $\tilde{N}(\omega)$  moved to infinity. In this case the main rise in  $1/\tau^{op}(\omega)$  is at  $\Omega_E + \Delta_{pg} \simeq 800 \text{ cm}^{-1}$ . Beyond this the curve rises approximately like  $[\omega - (\Omega_E + \Delta_{pg})]/\omega$  which is less rapid than the  $(\omega - \Omega_E)/\omega$  curve for the  $\Delta_{pg} = 0$  case.

The three remaining curves also have a pseudogap of  $550 \text{ cm}^{-1}$  but, in addition the lost state in  $\tilde{N}(\omega)$  are placed in the energy region just above  $\Delta_{pg}$  and state conservation is respected. This causes the scattering rate  $1/\tau^{op}(\omega)$  to rise much faster than in the dot-dashed curve because just above the gap we have more states to scatter into. The steepness of the rise depends on the distribution of states above  $\omega = \Delta_{pg}$ . The more the pileup is restricted in range the steeper the rise. Medium (purple), light (olive), and heavy (red) solid curves correspond, respectively to the case when the missing states are placed between  $\Delta_{pg}$  and  $2\Delta_{pg}$ ,  $1.5\Delta_{pg}$ , and  $1.1\Delta_{pg}$  (see inset in the top frame for the case  $1.5 \Delta_{pg}$  where the DOS is shown). Note also that the end of the recovery region in all cases is marked with a kink in  $1/\tau^{op}(\omega)$  after which the remaining rise is much more gradual and smooth. The features just described imply definite signatures in the corresponding real part of the optical self-energy as these are related by Kramers-Kronig (K-K) transform. The results for  $-\text{Im}\Sigma_1^{op}(\omega)$  based on Eq. 6 are shown in the top frame of Fig. 2. As is known from the work of Carbotte, Schachinger and Hwang [34]

the dashed (blue) curve would have a logarithmic singularity in slope at  $\omega = \Omega_E$  if we were using a pure delta function model and would have zero slope at  $\omega = \sqrt{2}\Omega_E$ . Similarly the dash-dotted (blue) curve would have infinite slope at  $\Omega_E + \Delta_{pg}$  and zero slope at  $\sqrt{2}(\Omega_E + \Delta_{pg})$ . These rules are very nearly satisfied in our model calculation even though we are using the spectra displayed in the inset lower frame rather than a pure delta function. We recall that the K-K transform of a sharp step like rise at  $\Omega_E$  and constant after this as applies to the quasiparticle scattering rate in a delta function model, has a logarithmic singularity at  $\omega = \Omega_E$ . The heavy (red) curve in the lower frame comes close to this case and indeed its K-K transform shows a sharp peak at this frequency reminiscent of a logarithmic singularity. We believe this to be the signature in the real part of the optical self-energy of pseudogap formation[29] as seen so prominently in the data of Fig. 1 for the two underdoped samples. A model with recovered DOS within  $\Delta_{pg}$  shows a clearly identifiable hat type structure in the medium solid (purple) curve for  $-2\Sigma_1^{op}(\omega)$  (Fig. 2 top frame) missing in both (blue) curves. This hat is perhaps not quite as sharp in this model calculation as it is in the data which is however less peaked than the heavy (red) curve. This indicates that the recovery region is consistent with a renormalized density of state for which the conservation of states occurs on the scale of  $\leq \Delta_{pg}$ .

Another interesting possibility to consider is the case when the pseudogap does not reduce  $\tilde{N}(\omega)$  to zero for  $\omega < \Delta_{pg}$  but rather still has a finite value. To illustrate this possibility, in the top left hand frame of Fig. 3, we show the imaginary part of  $\Sigma^{op}(\omega)$  for the case when the DOS is reduced to half its value rather than to zero below  $\Delta_{pg}$ . The light solid (olive) curve is to be compared with the heavy solid (red) curve which we reproduced from the bottom frame of Fig. 2. Both curves include full recovery in the energy interval  $\Delta_{pg}$  and  $2\Delta_{pg}$ . The light solid (olive) curve now starts at  $\omega = \Omega_E$  and has a step at  $\Omega_E + \Delta_{pg}$  after which it shows the characteristic sharp rise which we have associated with the density of state recovery region. In this case we see clear signatures of the resonance mode and of the pseudogap recovery region separately.

### 3. Effect of the pseudogap on real part of conductivity and on its partial sum rule

Having a model for the optical self-energy  $\Sigma^{op}(\omega)$ , we can calculate from it the real part of the conductivity. From Eq. 1 and the definitions of  $1/\tau^{op}(\omega)$  and  $\lambda^{op}(\omega)$  we get

$$\sigma_1(\omega) = \frac{\Omega_p^2}{4\pi} \frac{1/\tau^{op}(\omega)}{[\omega(1 + \lambda^{op}(\omega))]^2 + [1/\tau^{op}(\omega)]^2} \quad (10)$$

One point that needs to be made is that at zero temperature the inelastic optical scattering rate vanishes for  $\omega < \Omega_E$  in an Einstein model and the optical conductivity Eq. 10 becomes pathological:  $\sigma_1(\omega) = \Omega_p^2 \delta(\omega)/[4(1 + \lambda^{op}(0))]$  has a delta function at  $\omega = 0$  with weight reduced over the free electron case by  $1/(1 + \lambda)$ , where  $\lambda \equiv \lambda^{op}(0)$ , which coincides with the quasiparticle mass enhancement parameter  $\lambda^{qp}(\omega = 0)$  even for the case of an energy dependent density of state as we are considering here. . This

can be remedied by including a small amount of elastic impurity scattering as we did in Eq. 2. In this case  $1/\tau^{op}(\omega)$  around  $\omega = 0$  is a finite constant and its corresponding real part vanishes. Results for  $\sigma_1(\omega)$  vs.  $\omega$  are shown in the bottom frame of Fig. 3. In both cases  $1/\tau^{imp}$  is set equal to  $80 \text{ cm}^{-1}$  and  $\Omega_p$  is  $10000 \text{ cm}^{-1}$ . For the left hand frame we have used the  $I^2\chi(\omega)$  shown in the inset of the bottom frame of Fig. 2 which has an optical resonance as well as a background while for the right hand frame only the background is used. Starting with the left panel, the dashed (blue) curve clearly shows two regions, the Drude plus a Holstein boson assisted absorption piece which extends way beyond the Drude and mirrors the spectral density  $I^2\chi(\Omega)$ . For a delta function its onset is at  $\omega = \Omega_E$  and grows out of zero according to Eq. 10. It contains  $\lambda/(1 + \lambda)$  of the optical spectral weight. The remaining optical spectral weight  $1/(1 + \lambda)$  is to be found in the coherent Drude contribution. The width of the Drude is given very nearly by  $[1/\tau^{imp}(1 + \lambda)]$  which is different for the various curves because  $\lambda$  varies as we will explain. In the inset (bottom left frame) we repeat the solid (red) curve for pseudogap plus recovery and compare it with the same case but now the elastic scattering has been increased by a factor of 4. This fills in the region between Drude and Holstein processes much as is seen in the Bi-2212 data as one goes further into the underdoped region to  $T_c = 69 \text{ K}$ [31]. This can effectively switch some of the extra spectral weight that was transferred to the coherent part of the conductivity (Drude part) by the opening of the pseudogap back to the larger energies associated with the incoherent boson assisted part of the absorption (Holstein) region.

When there is no pseudogap as in the dashed (blue) curve, the quasiparticle mass enhancement parameter is given by

$$\lambda = 2 \int_0^\infty d\Omega \frac{I^2\chi(\Omega)}{\Omega} \quad (11)$$

If however a pseudogap is introduced it becomes modified and reads instead from Eq. 5 in the limit  $\omega \rightarrow 0$

$$\lambda = 2 \int_0^\infty d\omega' \tilde{N}(\omega') \int_0^\infty d\Omega \frac{I^2\chi(\Omega)}{(\omega' + \Omega)^2} \quad (12)$$

To remain simple we assume  $\tilde{N}(\omega) = t$  for  $\omega < \Delta_{pg}$  and  $2 - t$  for  $\omega \in (\Delta_{pg}, 2\Delta_{pg})$  and 1 beyond. That is, we have piled up the missing state equally in the interval  $\Delta_{pg}$  to  $2\Delta_{pg}$ . In this case the mass enhancement parameter becomes

$$\lambda = 2 \int_0^\infty d\Omega \frac{I^2\chi(\Omega)}{\Omega} h(\Omega) \quad (13)$$

with the modulating factor  $h(\Omega)$  equal to

$$h(\Omega) = \frac{2t + 3\Omega/\Delta_{pg} + (\Omega/\Delta_{pg})^2}{(1 + \Omega/\Delta_{pg})(2 + \Omega/\Delta_{pg})} \quad (14)$$

for the fully recovered case and

$$h(\Omega) = \frac{t + \Omega/\Delta_{pg}}{1 + \Omega/\Delta_{pg}} \quad (15)$$



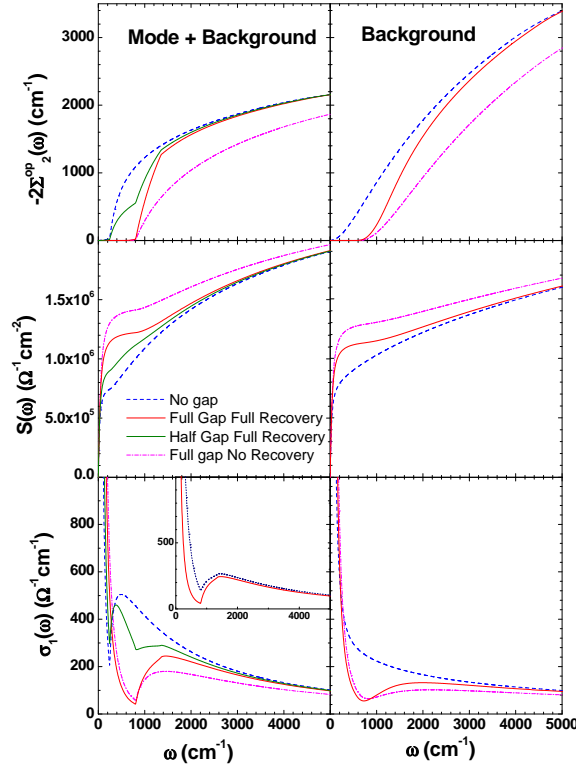


**Figure 3.** (color online) Model calculation of minus twice the imaginary part of the optical self-energy  $-2\Sigma_2^{op}(\omega)$  (top frame), the partial optical sum rule to energy  $\omega$  in units of  $\Omega^{-1}\text{cm}^{-2}$  (middle frame) and the real part (absorptive) of the optical conductivity in  $\text{cm}^{-1}$  (bottom frame) as a function of  $\omega$  in  $\text{cm}^{-1}$ . The curves on the left were calculated with the  $I^2\chi(\omega)$  shown in the inset of Fig. 2 while the right hand panel employed only the background contribution without a sharp optical resonance mode. Dashed (blue) curve is for no gap, dash-dotted (purple) for a gap without recovery, solid (red) for a gap with recovery, and light solid (olive) for a model in which only half the states are removed below the gap (with recovery). Inset same as solid (red) curve but with 4 times more elastic (impurity) scattering included.

for the case of no recovery region. This factor in effect reduces the low  $\Omega$  contribution to the mass enhancement factor from the spectral density alone. For a full pseudogap the suppression provides an extra factor of  $3\Omega/(2\Delta_{pg})$  and  $\Omega/\Delta_{pg}$  at small  $\Omega$  while for finite  $t$  it gives  $t + 3\Omega/(2\Delta_{pg})$  and  $t + \Omega/\Delta_{pg}$ , respectively. For the specific case considered here  $\lambda = 2.37$ , when we include a pseudogap Eq. 12 is reduced to 0.78 for a full gap with no recovery region above it and it is 1.06 when recovery is included as in Eq. 14. An unexpected consequence of this reduction in  $\lambda$  is that the Drude contribution (coherent part) to  $\sigma_1(\omega)$  is increased when a pseudogap is included and there is a corresponding decrease in the boson assisted Holstein (incoherent) contribution centered off  $\omega = 0$ . These factors translate into a wider Drude as  $\lambda$  is decreased. Dash-dotted (purple) is widest, then solid (red) and finally dashed (blue) at the same time the Holstein boson assisted region shows increasing weight from dash-dotted (purple) to solid (red) to dashed (blue) curves. Note also that a complete pseudogap below  $\omega = \Delta_{pg}$  cuts off the Holstein region which now starts at  $\omega = \Delta_{pg} + \Omega_E$  in the both solid (red) and

dash-dotted (purple) curves. The light solid (olive) curve is different from the others and shows two peaks rather than one in the Holstein region. It corresponds to an incomplete pseudogap with height  $t = 0.5$  at  $\omega = 0$ . This translates into a larger  $\lambda$  than for the solid (red) curve and its Drude peak indeed falls between (red) solid and (blue) dashed curves. Its Holstein region however starts at  $\Omega_E \simeq 250 \text{ cm}^{-1}$  (position of large peak in  $I^2\chi(\omega)$  of the inset in lower frame of Fig. 2) because the DOS is finite at the Fermi surface. This onset is followed by a peak with a second onset seen clearly at  $\omega = \Delta_{pg} + \Omega_E$  which corresponds to the sudden increase in the electronic DOS. To end this discussion of the effect of a pseudogap on the real (absorptive) part of the optical conductivity we consider the lower right hand panel of Fig. 3. Here only the background spectrum in  $I^2\chi(\omega)$  is included *i.e.* the delta function like optical resonance is excluded. We see that now Drude and Holstein contribution in the dashed (blue) curve are not clearly separated. While a two-contribution structure is seen in the other two curves these are not as well defined as in the corresponding curves of the left-hand panel. The existence of a sharp peak in electron-boson spectral density helps separate out the two distinct absorption processes (Drude and Holstein).

In the middle frame of Fig. 3 we show results for the partial optical sum  $S(\omega)$  defined as

$$S(\omega) = \int_0^\omega d\omega' \sigma_1(\omega'). \quad (16)$$

For  $\omega \rightarrow \infty$  in Eq. 16, we get the usual complete sum rule with  $S(\omega \rightarrow \infty) = \Omega_p^2/8$ . In our units this corresponds to  $\simeq 2.6 \times 10^6 \text{ cm}^{-2}$  with  $\Omega_p = 10000 \text{ cm}^{-1}$ . One sees clearly in these curves a rapidly increasing Drude contribution followed by a flattened region and then the Holstein contribution setting in at large values of  $\omega$ . The fraction of spectral weight seen in the Drude region is  $1/(1 + \lambda)$  of the total contribution. The remainder  $\lambda/(1 + \lambda)$  is the boson assisted contribution. If these two regions were truly separated in  $\sigma_1(\omega)$  the flattened region noted above would be perfectly flat. We make one more point about these results. In all cases there is, of course, conservation of optical spectral weight but this conservation occurs over a much larger frequency region for the real part of the conductivity than for the density of states itself which, in our model, is limited to the range 0 to  $2\Delta_{pg}$ . This is also true of the imaginary part of the optical self-energy but not for  $\sigma_1(\omega)$  or the partial sum  $S(\omega)$  of Eq. 15. Yu *et al.*[43] have recently noted this in their c-axis optical study of spectral weight redistribution due to the pseudogap.

Finally returning to the top frame of Fig. 3 we note that the sharp onset in scattering rate seen in the left-hand panel is considerably smeared out when the resonant peak in the boson spectral density  $I^2\chi(\omega)$  shown in the inset of the lower frame of Fig. 2 is left out and only the background spectral density is employed. This is shown in the right-hand panel (compare color coded curves).

#### 4. Conclusions

Motivated by the observation of hat like peak structures seen in the real part of the optical self-energy in underdoped cuprates which are absent in the overdoped case, we have considered a pseudogap model for their electronic structure consisting of a simple gap ( $\Delta_{pg}$ ) in the electronic DOS about the Fermi energy, with missing states recovered in the energy region right above it. This simple model augmented with an optical peak in the electron-boson spectral density is remarkably successful in describing the data and is further used to describe other optical quantities. The optical scattering rate, the real part of the conductivity and its partial sum are considered as is the derivative of  $\Sigma_1^{op}(\omega)$ . These quantities all show specific signatures of the pseudogap. While the redistribution of electronic states in the DOS is limited to the region  $\omega \leq 2\Delta_{pg}$  we found that the corresponding redistribution of optical spectral weight in the real part of the conductivity is spread over a much large range. This is also true for the real part of the optical self-energy but not for its imaginary part for which the important changes due directly to the opening of pseudogap are confined much more to the range  $\omega \leq 2\Delta_{pg}$ . Comparing results of model calculations we conclude that pseudogap effects can be readily distinguished from the effect of multiple peaks in the electron-boson spectral density  $I^2\chi(\omega)$ .

#### Acknowledgments

This work has been supported by the Natural Science and Engineering Research Council of Canada and the Canadian Institute for Advanced Research.

#### References

- [1] Timusk T and Statt B 1999 *Rep. Prog. Phys.* **62** 61
- [2] Zasadzinski J F, Ozyuzer L, Miyakawa N, Gray K E, Hinks D G and Kendziora C 2001 *Phys. Rev. Lett.* **87** 067005
- [3] Sutherland Mike, Hawthorn D G, Hill R W, Ronning F, Wakimoto S, Zhang H, Proust C, Boaknin Etienne, Lupien C and Taillefer Louis 2003 *Phys. Rev. B* **67** 174520
- [4] Emery V J and Kivelson S A 1995 *Nature (London)* **374** 434
- [5] Krasnov V M, Yurgens A, Winkler D, Delsing P, and Claeson T 2000 *Phys. Rev. Lett.* **84** 5860
- [6] Le Tacon M, Sacuto A, Georges A, Kotliar G, Gallais Y, Colson D and Forget A 2006 *Nature Physics* **2** 537
- [7] Kanigel A, Norman M R, Randeria M, Chatterjee U, Souma S, Kaminski A, Fretwell H M, Rosenkranz S, Shi M, Sato T, Takahashi T, Li Z Z, Raffy H, Kadowaki K, Hinks D, Ozyuzer L and Campuzano J C 2006 *Nature Physics* **2** 447
- [8] Warren Jr W W, Walstedt R E, Brennert G F, Cava R J, Tycko R, Bell R F and Dabbagh G 1989 *Phys. Rev. Lett.* **62** 1193
- [9] Homes C C, Timusk T, Liang R, Bonn D A and Hardy W N 1993 *Phys. Rev. Lett.* **71** 1645
- [10] Loram J W, Mirza K A, Cooper J R and Tallon J L 1998 *J. Phys. Chem. Solids* **59** 2091
- [11] Loram J W, Luo J, Cooper J R, Liang W Y and Tallon J L 2001 *J. Phys. Chem. Solids* **62** 59
- [12] Renner Ch, Revaz B, Genoud J -Y, Kadowaki K and Fischer O 1998 *Phys. Rev. Lett.* **80** 149
- [13] Chakravarty S, Laughlin R P, Morr D K and Nayak C 2001 *Phys. Rev. B* **63** 094503

- [14] Dora B, Virosztek A and Maki K 2002 *Phys. Rev. B* **65** 155119 ; Maki K, Dora B, Kartsovnik M, Virosztek A, Korin-Hamzic B and Basletic M 2003 *Phys. Rev. Lett.* **90** 256402
- [15] Chakravarty S, Kee H -Y and Nayak C 2001 *Int. J. Mod. Phys. B* **15** 2901
- [16] Zhu J -X, Kim W, Ting C S and Carbotte J P 2001 *Phys. Rev. Lett.* **87** 197001
- [17] Yang X and Nayak C 2002 *Phys. Rev. B* **65** 064523
- [18] Wang Q H, Han J H and Lee D H 2001 *Phys. Rev. Lett.* **87** 077004
- [19] Chakravarty S, Nayak C, Tewari S and Yang X 2002 *Phys. Rev. Lett.* **89** 277003
- [20] Capelutti E and Zehyer R 1999 *Phys. Rev. B* **59** 6475
- [21] Benfatto L, Caprara S and C. DiCastro C 2000 *Eur. Phys. J. B* **17** 95
- [22] Aristov D N and Zeyher R 2004 *Phys. Rev. B* **70** 212511
- [23] Valenzuela B, Nicol E J and Carbotte J P 2005 *Phys. Rev. B* **71** 134503
- [24] Kim W and Carbotte J P 2002 *Phys. Rev. B* **66** 033104
- [25] Kim W, Zhu J X, Carbotte J P and Ting C S 2002 *Phys. Rev. B* **65** 064502
- [26] Benfatto L and Sharapov S 2006 *Low Temp. Phys.* **32** 533
- [27] Aristov D N and Zeyher R 2005 *Phys. Rev. B* **72** 115118
- [28] Gerami R and Nayak C 2006 *Phys. Rev. B* **73** 024505
- [29] Hwang J, Carbotte J P and Timusk T 2007 submitted to *Phys. Rev. Lett.*
- [30] Hwang J, Timusk T and Gu G D 2004 *Nature (London)* **427** 714
- [31] Hwang J, Timusk T and Gu G D 2007 *J. Phys.: Condens. Matter* **19** 125208
- [32] Hwang J, Yang J, Timusk T, Sharapov S G, Carbotte J P, Bonn D A, Liang Ruixing and Hardy W N 2006 *Phys. Rev. B* **73** 014508
- [33] Marsiglio F and Carbotte J P 2003 in "The Physics of Superconductors: Conventional and Unconventional" edited by Bennemann K H and Ketterson J B, Springer p.233
- [34] Carbotte J P, Schachinger E and Hwang J 2005 *Phys. Rev. B* **71** 054506
- [35] Mitrovic B and Carbotte J P 1983 *Can. J. Phys.* **61** 758 ; 1983 *ibid* **61** 784
- [36] Mitrovic B and Fiorucci M A 1985 *Phys. Rev. B* **31** 2694
- [37] Knigavko A and Carbotte J P 2005 *Phys. Rev. B* **72** 035125
- [38] Knigavko A and Carbotte J P 2006 *Phys. Rev. B* **73** 125114
- [39] Sharapov S G and Carbotte J P 2005 *Phys. Rev. B* **72** 134506
- [40] Hwang J, Nicol E J, Timusk T, Knigavko A and Carbotte J P 2007 *Phys. Rev. Lett.* **98** 207002
- [41] Allen P B 1971 *Phys. Rev. B* **3** 305
- [42] Shulga S V, Dolgov O V and Maksimov E G 1991 *Physica C* **178** 266
- [43] Yu Li, Munzar D, Boris A V, Yordanov P, Chaloupka J, Wolf Th, Lin C T, Keimer B and Bernhard C 2007 (*preprint cond-mat/0705.0111*)